Figure S1

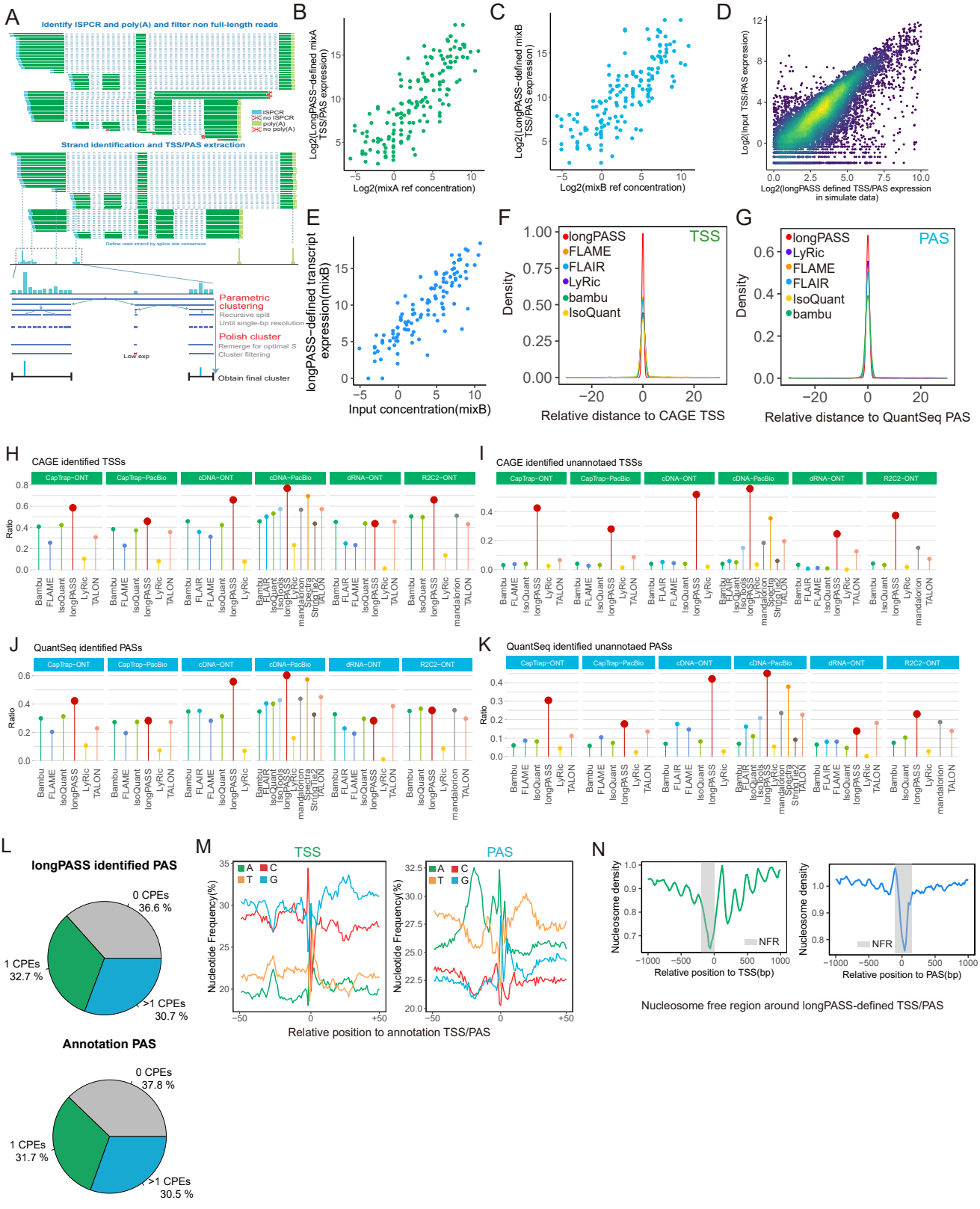
A
Identify ISPCR and poly(A) and filter non full-length reads
ISPCR
no ISPCR
poly(A)
no poly(A)
Strand identification and TSS/PAS extraction
Define read strand by splice site consensus
Parametric clustering
Recursive split
Until single-bp resolution
Polish cluster
Remerge for optimal S
Cluster filtering
Low exp
Obtain final cluster
B
Log2(LongPASS−defined mixA TSS/PAS expression)
Log2(mixA ref concentration)
C
Log2(LongPASS−defined mixB TSS/PAS expression)
Log2(mixB ref concentration)
D
Log2(Input TSS/PAS expression)
Log2(longPASS defined TSS/PAS expression in simulate data)
E
longPASS−defined transcript expression(mixB)
Input concentration(mixB)
F
longPASS
FLAME
FLAIR
LyRic
bambu
IsoQuant
TSS
Density
Relative distance to CAGE TSS
G
longPASS
LyRic
FLAME
FLAIR
IsoQuant
bambu
PAS
Density
Relative distance to QuantSeq PAS
H
CAGE identified TSSs
CapTrap−ONT
CapTrap−PacBio
cDNA−ONT
cDNA−PacBio
dRNA−ONT
R2C2−ONT
Ratio
I
CAGE identified unannotaed TSSs
J
QuantSeq identified PASs
K
QuantSeq identified unannotaed PASs
L
longPASS identified PAS
0 CPEs 36.6 %
1 CPEs 32.7 %
>1 CPEs 30.7 %
Annotation PAS
0 CPEs 37.8 %
1 CPEs 31.7 %
>1 CPEs 30.5 %
M
TSS
PAS
A
C
T
G
Nucleotide Frequency(%)
Relative position to annotation TSS/PAS
N
Nucleosome density
NFR
Relative position to TSS(bp)
Relative position to PAS(bp)
Nucleosome free region around longPASS-defined TSS/PAS

Figure S1. LongPASS TSS/PAS clustering and validation, related to Fig.1. (A) Workflow for longPASS clustering TSS/PAS from long-read sequencing data. **(details see methods)**. **(B-C).** Correlation between annotated and longPASS-defined TSS/PAS expression of RNA sequins (left panel mix A, Pearson correlation coefficient = 0.8(B); right panel mix B, Pearson correlation coefficient = 0.82(C)). **(D).** Correlation between input TSS/PAS TPM and TSS/PAS TPM identified by longPASS in *NanoSim* simulated data. and longPASS-defined isoform expression of RNA sequins (mix B, Pearson correlation coefficient = 0.88). **(E).** Correlation between annotated and longPASS-defined isoform expression of RNA sequins (mix B, Pearson correlation coefficient = 0.88). **(F, G)** Distance between TSS(F) and PAS(G) defined by longPASS and other long-read analysis methods to CAGE-detected TSS or QuantSeq detected PAS. **(H, I, J, K)** Sensitivity of longPASS Versus Other Long-Read Analysis Methods in Identifying CAGE-defined TSSs **(H)**, CAGE-defined unannotated TSSs **(I)**, QuantSeq-defined PASs **(J)**, QuantSeq-defined unannotated PASs **(K)**. **(L)** Comparison of CPE signal enrichment within ±100 bp regions surrounding PASs defined by longPASS or from the reference genome **(M).** Nucleotide composition around reference genome (Gencode v38) annotated TSS/PAS. **(N)** Nucleosome density revealed by MNase-Seq around longPASS-defined TSS/PAS. Shaded area represents nucleosome free region (NFR).

Figure S2

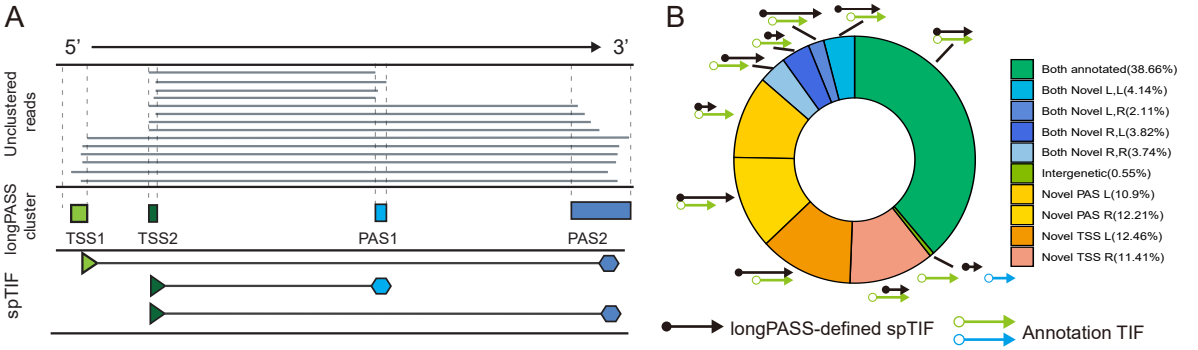
A
5'
3'
Unclustered reads
longPASS cluster
TSS1
TSS2
PAS1
PAS2
spTIF
B
Both annotated(38.66%)
Both Novel L,L(4.14%)
Both Novel L,R(2.11%)
Both Novel R,L(3.82%)
Both Novel R,R(3.74%)
Intergenetic(0.55%)
Novel PAS L(10.9%)
Novel PAS R(12.21%)
Novel TSS L(12.46%)
Novel TSS R(11.41%)
longPASS-defined spTIF
Annotation TIF

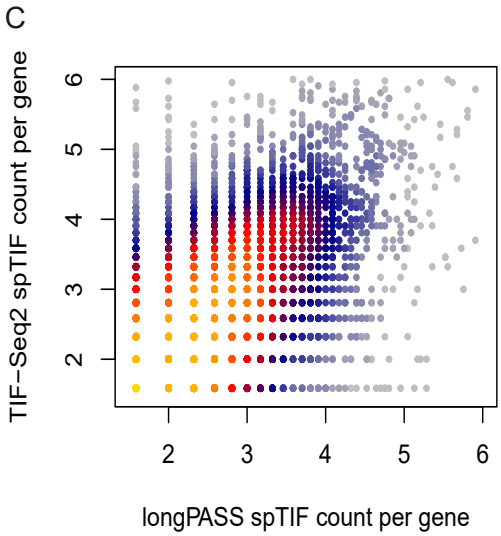
C
TIF−Seq2 spTIF count per gene
longPASS spTIF count per gene
2
3
4
5
6

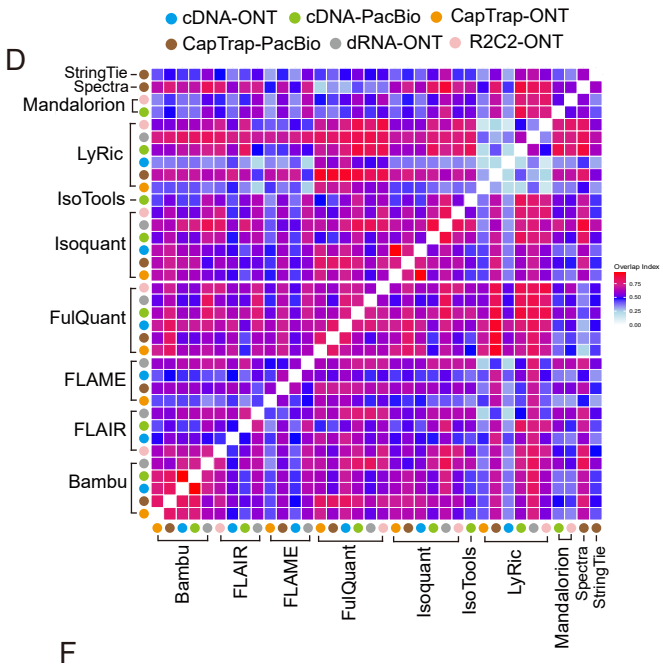
D
cDNA-ONT
cDNA-PacBio
CapTrap-ONT
CapTrap-PacBio
dRNA-ONT
R2C2-ONT
StringTie
Spectra
Mandalorion
LyRic
IsoTools
Isoquant
FulQuant
FLAME
FLAIR
Bambu
Overlap Index

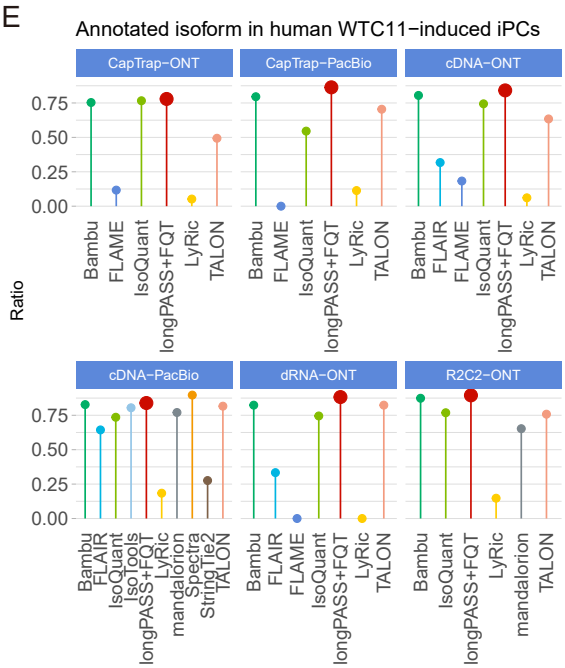
E
Annotated isoform in human WTC11−induced iPCs
CapTrap−ONT
CapTrap−PacBio
cDNA−ONT
cDNA−PacBio
dRNA−ONT
R2C2−ONT
Ratio
0.00
0.25
0.50
0.75
Bambu
FLAIR
FLAME
IsoQuant
IsoTools
longPASS+FQT
LyRic
mandalorion
Spectra
StringTie2
TALON

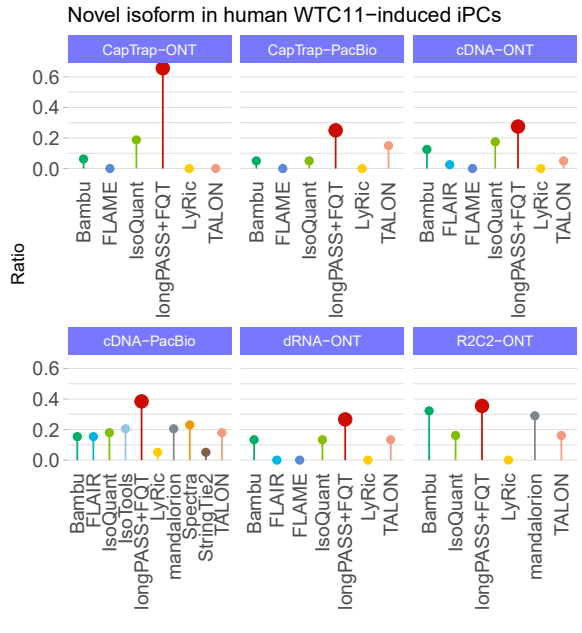
F
Novel isoform in human WTC11−induced iPCs
CapTrap−ONT
CapTrap−PacBio
cDNA−ONT
cDNA−PacBio
dRNA−ONT
R2C2−ONT
Ratio
0.0
0.2
0.4
0.6
Bambu
FLAIR
FLAME
IsoQuant
IsoTools
longPASS+FQT
LyRic
mandalorion
Spectra
StringTie2
TALON

Figure S2. LongPASS helps isoform definition, related to Fig.1. (A) Diagram showing construction of spTIFs by linking longPASS-defined TSS and PAS. **(B)** Classification and proportion of longPASS-defined spTIFs, according to comparison with the gencode annotation transcripts. **(C)** Correlation between TIF-Seq2 defined and longPASS-defined spTIF log2 count per gene (Pearson correlation coefficient =0.55). **(D)** UIC consistence of FulQuant compared to other methods across different long-read protocols. **(E, F)** Sensitivity of isoform detection in WTC11-Induced human iPCs by integrating longPASS and FulQuant compared to other Methods: Annotated Isoforms **(E)**, Novel Isoforms **(F)**

Figure S3

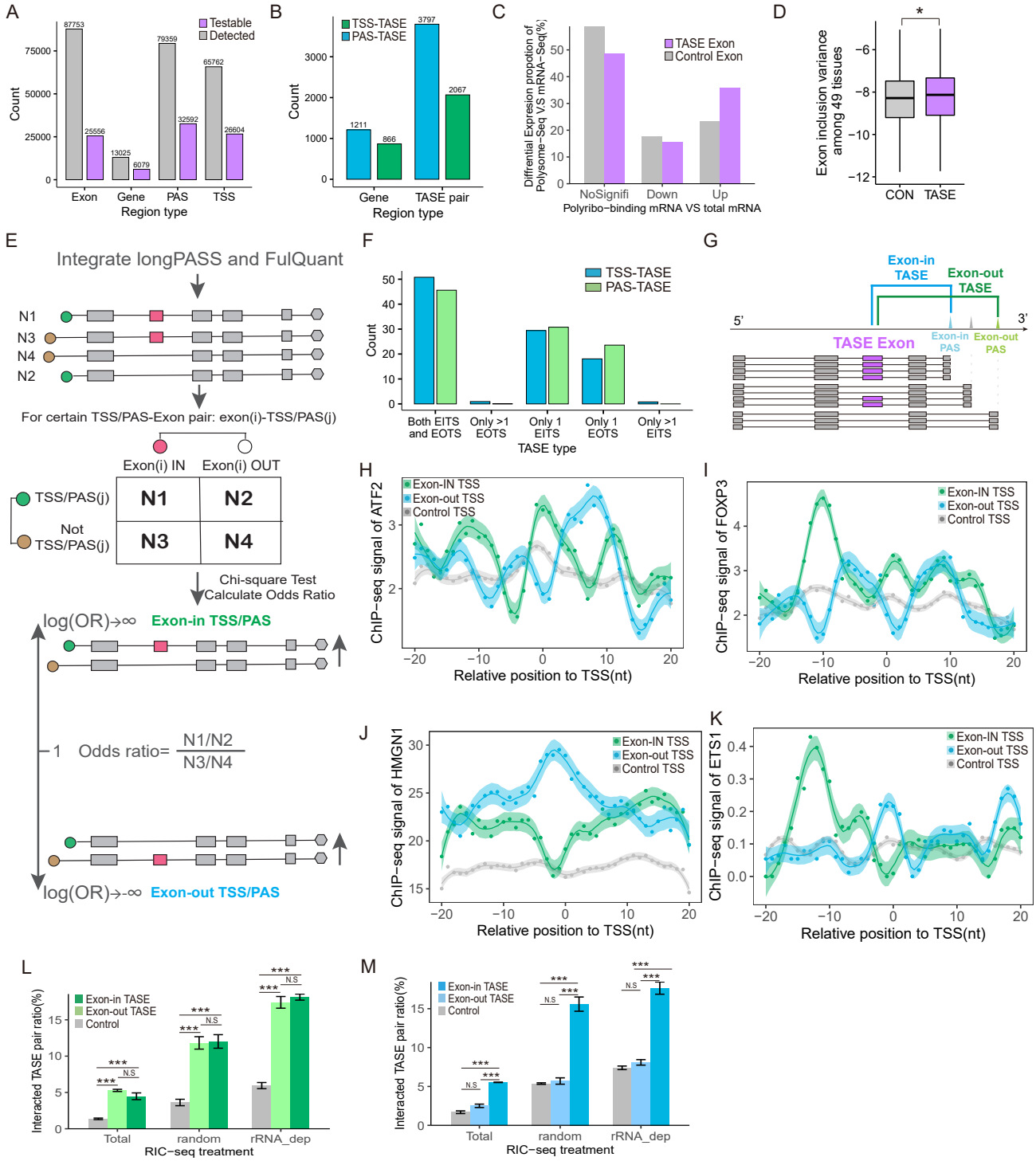
A
Testable
Detected
Count
Exon
Gene
PAS
TSS
Region type
B
TSS-TASE
PAS-TASE
Count
Gene
TASE pair
Region type
C
TASE Exon
Control Exon
Diffrential Expresion propotion of Polysome−Seq VS mRNA−Seq(%)
NoSignifi
Down
Up
Polyribo−binding mRNA VS total mRNA
D
Exon inclusion variance among 49 tissues
CON
TASE
E
Integrate longPASS and FulQuant
N1
N3
N4
N2
For certain TSS/PAS-Exon pair: exon(i)-TSS/PAS(j)
Exon(i) IN
Exon(i) OUT
TSS/PAS(j)
Not TSS/PAS(j)
N1
N2
N3
N4
Chi-square Test
Calculate Odds Ratio
log(OR)→∞
Exon-in TSS/PAS
Odds ratio= N1/N2 / N3/N4
log(OR)→-∞
Exon-out TSS/PAS
F
TSS-TASE
PAS-TASE
Count
Both EITS and EOTS
Only >1 EOTS
Only 1 EITS
Only 1 EOTS
Only >1 EITS
TASE type
G
Exon-in TASE
Exon-out TASE
5'
3'
TASE Exon
Exon-in PAS
Exon-out PAS
H
Exon-IN TSS
Exon-out TSS
Control TSS
ChIP−seq signal of ATF2
Relative position to TSS(nt)
I
Exon-IN TSS
Exon-out TSS
Control TSS
ChIP−seq signal of FOXP3
Relative position to TSS(nt)
J
Exon-IN TSS
Exon-out TSS
Control TSS
ChIP−seq signal of HMGN1
Relative position to TSS(nt)
K
Exon-IN TSS
Exon-out TSS
Control TSS
ChIP−seq signal of ETS1
Relative position to TSS(nt)
L
Exon-in TASE
Exon-out TASE
Control
Interacted TASE pair ratio(%)
Total
random
rRNA_dep
RIC−seq treatment
M
Exon-in TASE
Exon-out TASE
Control
Interacted TASE pair ratio(%)
Total
random
rRNA_dep
RIC−seq treatment

Figure S3. TASEs exhibit distinct characteristics compared to controls, related to Fig.2. (A). Number of regions detected in this analysis and testable regions for TASE coupling test. **(B).** Statistics of identified TASE pairs and associated gene count. **(C)** Differential expression of Exons (TASEs vs Control) in Ribo-seq vs. total mRNA-seq data ('Up' indicates exons with significantly higher ribosome levels relative to transcriptional levels, opposite relationship labeled 'Down'). **(D)** Exon inclusion variance across 49 tissues (GTEx), TASE (n = 3,154) versus Control (n = 12,000), **P* = 0.011, *P* value from two-tailed Mann-Whitney test. **(E)** Diagram showing steps for distinguishing Exon-in TASEs and Exon-out TASEs. **(F).** Statistics of TASE type associated with each TASE exon (Exon-in-TSS/PAS, Exon-out-TSS/PAS). **(H-I)** Transcription factors that show differential binding signal around different types of TSS. **(J-K).** The proportion of spatially interacting TSS-exon pairs (J) or PAS-exon pairs (K) from different groups revealed by RIC-Seq with different library method.

Figure S4

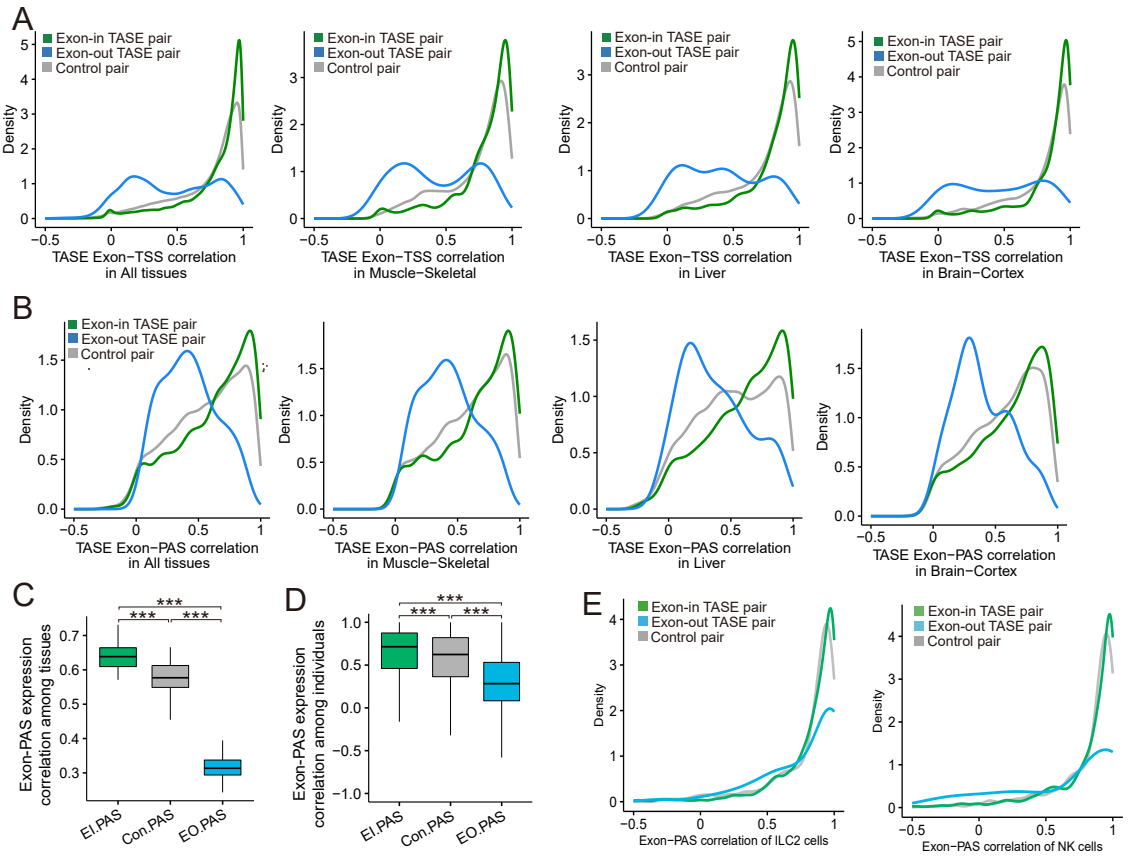

Figure S4. TASE is a pervasive way of gene regulation, related to Fig.3. (A) Correlation distribution of TASE TSS-Exon pairs in all tissues, and individual tissues (Liver, Brain-cortex, Muscle-skeletal). **(B)** Correlation distribution of TASE Exon-PAS pairs in all tissues, and individual tissues (Liver, Brain-cortex, and Muscle-skeletal). **(C).** Comparing the expression correlation of different kinds of TASE Exon-PAS pairs across 49 different tissues. **(D)** Comparing the expression correlation of different kinds of TASE Exon-PAS pairs across 838 different human individuals. **(E)** Correlation distribution of TASE Exon-PAS pairs in ILC2 cell and NK cell.

Figure S5

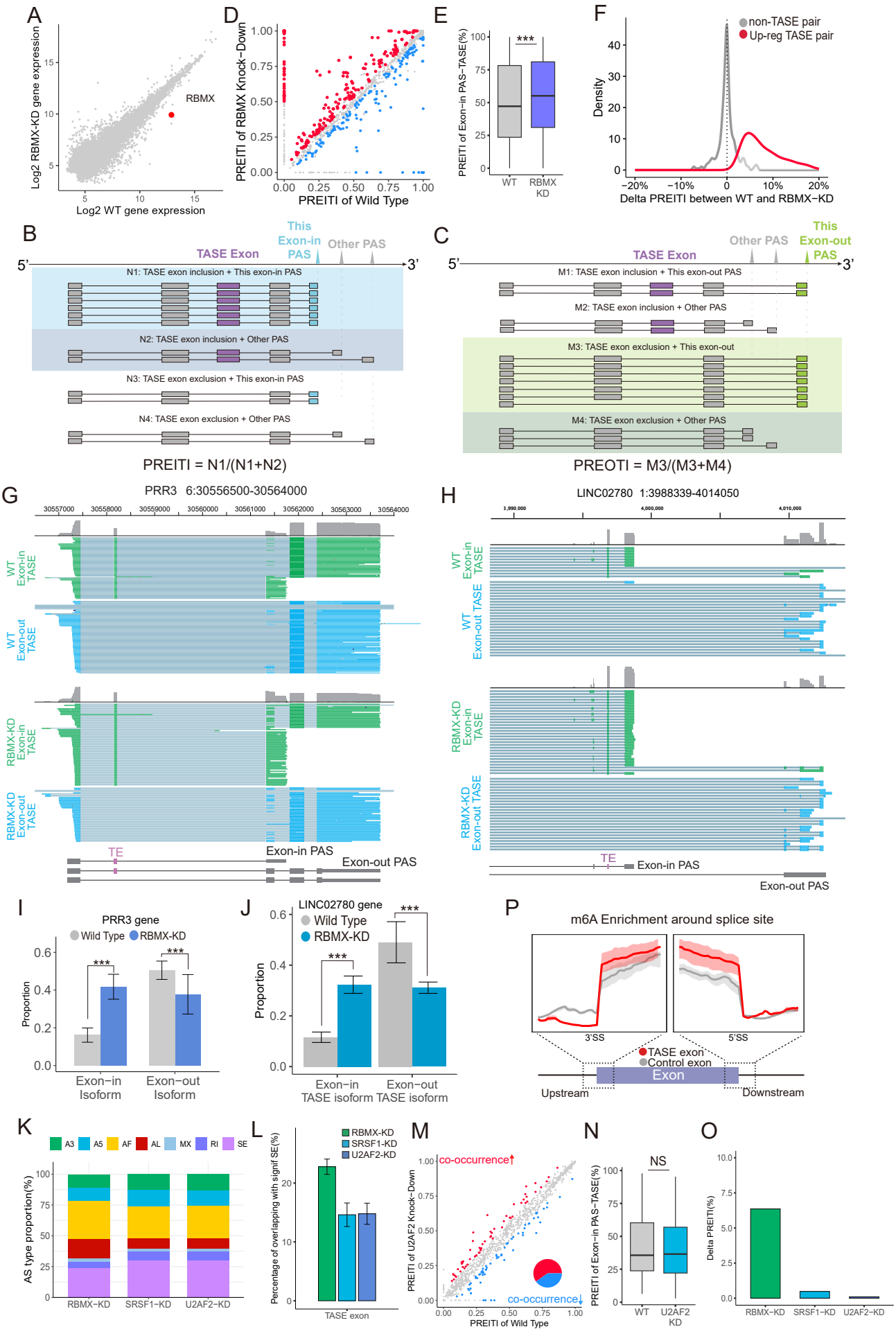
A
Log2 RBMX-KD gene expression
Log2 WT gene expression
RBMX
D
PREITI of RBMX Knock−Down
PREITI of Wild Type
E
PREITI of Exon−in PAS−TASE(%)
***
WT
RBMX KD
F
non-TASE pair
Up-reg TASE pair
Density
Delta PREITI between WT and RBMX−KD
B
TASE Exon
This Exon-in PAS
Other PAS
5'
3'
N1: TASE exon inclusion + This exon-in PAS
N2: TASE exon inclusion + Other PAS
N3: TASE exon exclusion + This exon-in PAS
N4: TASE exon exclusion + Other PAS
PREITI = N1/(N1+N2)
C
TASE Exon
Other PAS
This Exon-out PAS
M1: TASE exon inclusion + This exon-out PAS
M2: TASE exon inclusion + Other PAS
M3: TASE exon exclusion + This exon-out
M4: TASE exon exclusion + Other PAS
PREOTI = M3/(M3+M4)
G
PRR3 6:30556500-30564000
WT Exon-in TASE
WT Exon-out TASE
RBMX-KD Exon-in TASE
RBMX-KD Exon-out TASE
TE
Exon-in PAS
Exon-out PAS
H
LINC02780 1:3988339-4014050
WT Exon-in TASE
WT Exon-out TASE
RBMX-KD Exon-in TASE
RBMX-KD Exon-out TASE
TE
Exon-in PAS
Exon-out PAS
I
PRR3 gene
Wild Type
RBMX-KD
Proportion
***
Exon−in Isoform
Exon−out Isoform
J
LINC02780 gene
Wild Type
RBMX-KD
Proportion
***
Exon−in TASE isoform
Exon−out TASE isoform
P
m6A Enrichment around splice site
3'SS
5'SS
TASE exon
Control exon
Exon
Upstream
Downstream
K
A3
A5
AF
AL
MX
RI
SE
AS type proportion(%)
RBMX−KD
SRSF1−KD
U2AF2−KD
L
RBMX-KD
SRSF1-KD
U2AF2-KD
Percentage of overlapping with signif SE(%)
TASE exon
M
co-occurrence↑
co-occurrence↓
PREITI of U2AF2 Knock−Down
PREITI of Wild Type
N
NS
PREITI of Exon−in PAS−TASE(%)
WT
U2AF2 KD
O
Delta PREITI(%)
RBMX−KD
SRSF1−KD
U2AF2−KD

Figure S5. Knocking down RBMX impacts TASE co-regulation, related to Fig.4. (A) The expression of genes in RBMX knock-down experiment vs. control. **(B-C)** The Calculation of PREITI and PREOTI. **(D)** The comparison of PREITI (Percentage of Exon-in-TASE isoform Index) for Exon-in-PAS-TASEs in RBMX knock-down (RBMX-KD) and WT cells. PREITI significantly (|PREITI| > 0.1, P<0.001) increased cases are colored red, and decreased cases are colored blue. **(E)** Boxplot of PREITI scores for significant Exon-in-PAS-TASE in (D) of RBMX knock-down and WT cells**. (F)** The density distribution of delta PREITIs between RBMX-KD and WT for up-regulated Exon-in-PAS TASE pairs (red) and non-TASE controls (grey). **(G).** The alignment of raw long reads of Exon-in and Exon-out-PAS-TASE isoforms from the *PRR3* gene in RBMX-KD and WT cells, Exon-in: ****P*< 3.9e-4, Exon-out: **P*<0.0413. *P* from two-proportions *z*-test and FDR correction applied. **(H).** The alignment of raw long reads of Exon-in and Exon-out-PAS-TASE isoforms in *LINC02780* gene for RBMX-KD and WT cells. **(I-J)**. The proportion of long reads of TASE Exon-in and Exon-out isoforms in *PRR3* gene **(I)** and LINC02780 and *LINC02780* gene **(J)** for RBMX-KD and WT cells. **(K)** Proportional Distribution of Significant Alternative Splicing Event Types Identified by SUPPA (A5: alternative 5'SS, A3: alternative 3'SS, AF: alternative first exon, AL: alternative last exon, MX: mutual exclusive exon, RI: Intron retention, SE: exon skipping). **(L)** Proportion of TASE Exons Overlapping with Significantly Skipped Exons Under Each KD Condition. **(M)** Comparison of PREITI of Exon-in-PAS-TASEs (n=1963) between U2AF2-KD and WT cells. Significant PREITI (|PREITI| > 0.07, *P*<0.001) increases are colored red and decreases are colored blue. **(N)** Boxplot of PREITIs for significant Exon-in-PAS-TASEs in U2AF2-KD and WT cells**. (O)** Change in PREITI (ΔPREITI) of Significant Exon-in PAS TASE Events Compared to WT Across Different Knockdown Conditions**. (P)** The m6A signals around acceptor and donor splice sites of PAS-TASE (n=2148) and control exons (n=12000).

Figure S6

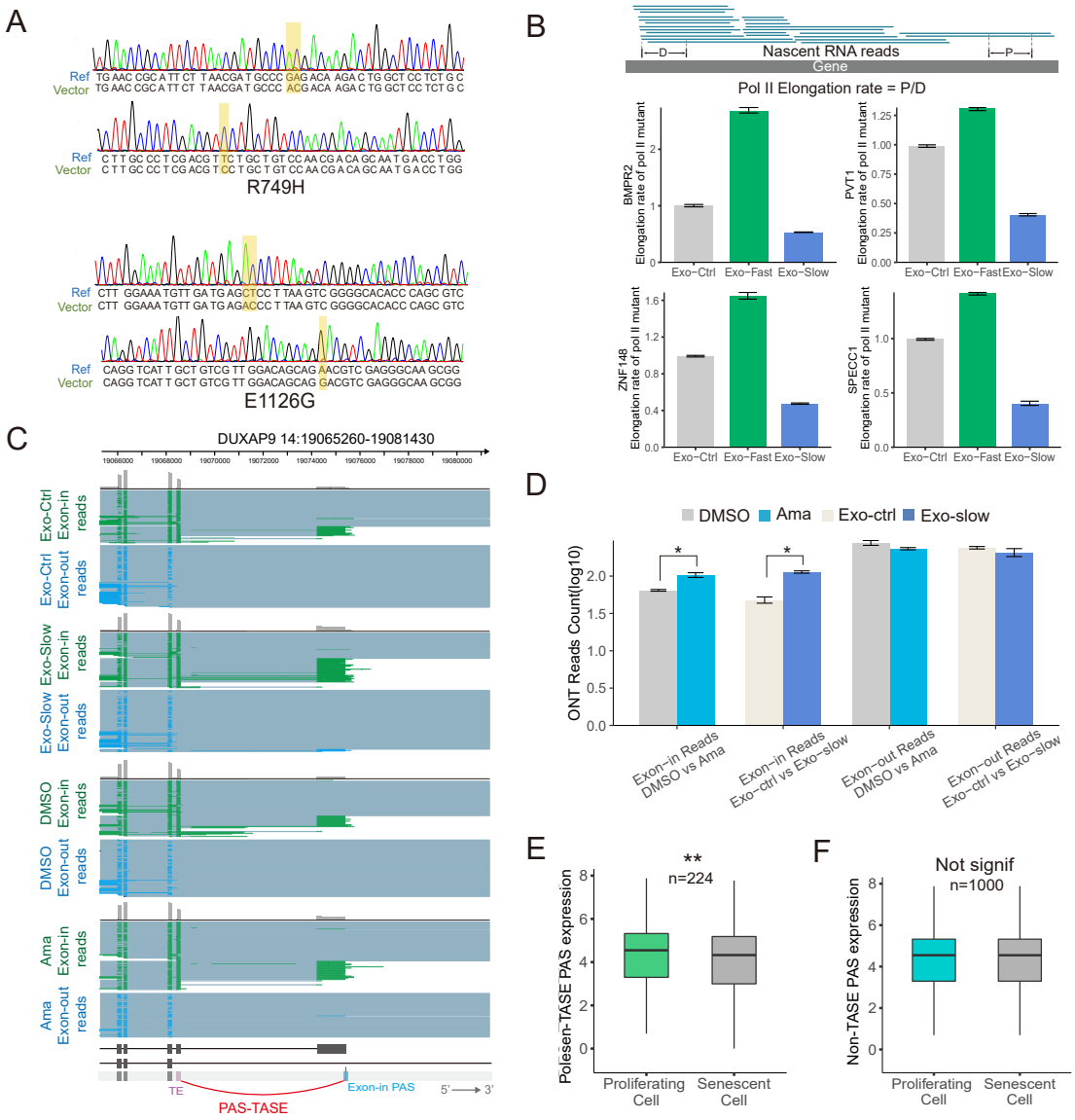

Figure S6. Altered Pol II elongation rate impacts TASE co-regulation, related to Fig.5. (A). Sanger-Seq demonstrating mutation (R749H, E1126G) on associated 293T Pol II mutant. **(B)** Validating the Pol II elongation speed of each mutant using nascent RNA methods (P: proximal region, D: distal region; P/D are used to evaluate elongation rate), measured by qPCR, conducted with three technical replicates. **(C)** ONT raw reads of PAS-TASE case of *DUXAP9* in Exo-ctrl, Exo-slow, DMSO and Ama. **(D)** Statistics of TASE-related region expression of *DUXAP9* in Exo-ctrl, Exo-slow, DMSO and Ama (each n = 2). **(E-F)**. Comparison of PoleSen-PAS and non-TASE PAS between proliferating state and senescent state of HUVECs.